Synchronization of Microgrid Considering the Dynamics of V2Gs Using an Optimized Fractional Order Controller based Scheme

A. Khorshidi, T. Niknam*, B. Bahmani

Department of Electrical Engineering, Marvdasht Branch, Islamic Azad University, Marvdasht, Iran

Abstract- *In this work, a new control scheme for synchronization of AC microgrids with upstream power grid is presented. The effects of V2Gs (vehicle to grid) dynamics on synchronization process is studied. This new control approach is based on the optimal fractional calculus and has been developed for synchronization of the microgrid. The V2Gs effect on the dynamics of the microgrid is analyzed through small signal stability and simulations. This effect is also considered in synchronization process by considering a PHEV-dominated-microgrid. The proposed control scheme is a coordinated control of distributed resources and provides a soft and reliable synchronization for microgrid. In the proposed control scheme, the fractional order proportional-integral-derivative (FOPID) controllers have optimally been tuned and implemented using the genetics algorithm (GA). The simulation results confirm the effectiveness of the proposed control strategy in soft and swift synchronization of the microgrid.*

Keyword: Microgrid, synchronization, FOPID, V2G.

NOMENCLATURE

DG	Distributed Generation
V2G	Vehicle to Grid
PV	Photovoltaic system
PHEV	Plug-in Electric Vehicle
FOPID	Fractional Order Proportional Integral Derivative controller
DFT	Discrete Fourier Transform
GA	Genetic Algorithm
RES	Renewable Energy Resource
MPPT	Maximum Power Point Tracking
AVR	Automatic Voltage Regulator
ICE	Internal Combustion Engine
TSC	Taylor Series Expansion
PCC	Point of Common Coupling

1. INTRODUCTION

Nowadays, the renewable energy resources (RESs) and distribution generations (DGs) have been penetrated in conventional power system because of reduction in fossil fuels, increasing energy demand, economic aspects and environmental problems of the traditional fossil fuel-based energy resources [1]. A rational and

effective way to integrate and control these resources, accompanied with related loads, is to implement them in a small framework called the microgrid. In the view of bulk power grid, the microgrid is a low-voltage controllable load that is able to interact with the power grid [2]. There are many advantages in employing the microgrid such as reliability improvement, air pollution reduction and economical aspects [3]-[5]. A microgrid, generally, contains different types of RESs, e.g. wind energy, diesel generators, photovoltaic (PV) units, PHEVs, and also energy storage systems, e.g. batteries, flywheel, super capacitors…, and electrical and non-electrical loads. All of these elements must be coordinated and controlled in an appropriate method in order to enable the microgrid operate normally. The microgrid mode of operation, however, is also an important aspect in microgrid control. Commonly, to interchange active and reactive powers with the power grid, the microgrid operates in grid-connected mode. Depending upon the control strategy, in this mode of operation, the voltage and frequency of the microgrid are imposed by the power grid [6]. However, there are some cases in which the microgrid must be disconnected from the power grid and operate in stand-alone mode or islanded mode [7]. In this case, the microgrid supplies the local loads and individually controls the voltage and frequency.

For synchronization of the microgrid with the main power grid many approaches have been reported in literature. In Ref. [12], the frequency deviation is

reduced using a zero-crossing method that detects the zero-passing instant of the voltages of microgrid and utility. However, it suffers weak dynamic performance when the grid voltage has harmonic components [13]. Many researchers have tried to improve this method by adjusting the zero-passing technique [14] or using Discrete Fourier Transform (DFT) [15]. The latter has reported to be sturdy against harmonics, however, it suffers from time delay during sampling process [16]. In Ref. [17], a collection of different microgrids has been modeled as a Kuramoto model of phase-coupled oscillators. This approach is taken to synchronize microgrids and the characteristics of the whole model was investigated. Nevertheless, the method is based on the simple constant voltage assumption. A linear Kalman filter was designed in Ref. [18] that uses phase-locked-loop (PLL) to synchronize he microgrid with utility. This method suffers from poor reliability in the case of failure in main communication links. In Ref. [19], for synchronization of islanded microgrid, proportional-integral (PI) controller-based method was proposed. However, the controllers were not optimally tuned and the method was weak when introducing the large communication delays. The method introduced in Ref. [20], adopted a linear-time invariant model for microgrid and take a cooperative control approach for synchronization. The controllers were optimally tuned using the consensus algorithm. However, the blind spot of this method was its weakness against system uncertainties. The authors of [21] proposed a robust control approach based on H∞ theory. However, during the failure of central controller, the performance of the method is deteriorated.

Nowadays, fractional order PID (FOPID) controllers are getting more interests in industrial applications due to their time/frequency domain specifications such as robustness, well-tuned capability, and lower over-shoot and settling time. These characteristics have been confirmed in many applications such as electrical drives [22-23], photovoltaic systems [24], low frequency control and automatic voltage control in power systems [25-26]. The present study aims to design and verify the performance of the optimal FOPID intended for synchronization of microgrid with main power grid. The FOPID has been optimally tuned using the genetics algorithm (GA). The main contributions of this paper are as follows:

- The effects of PHEVs have also been considered during synchronization.

- A new control strategy for synchronization of

microgrid with utility is presented. The proposed strategy is a coordinated control of distributed resources and provides a soft and reliable synchronization for microgrid.

The rest of the paper is organized as follows: Section 2 introduce the overall structure of the microgrid and dynamic model of each distributed energy resource, especially, the PHEVs. The impact of PHEVs on the microgrid dynamics is analyzed in Section 3. The designing procedure of the optimal FOPID controller is described in Section 4. The performance of the proposed control strategy is analyzed through simulation studies in Section 5. Finally, the conclusion is given in Section 6.

2. STRUCTURE OF THE MICROGRID AND MATHEMATICAL MODELS

Overall block diagram of the microgrid is demonstrated in Fig. 1. The microgrid contains a diesel generator, a parking lot that contains integrated PHEVs, photovoltaic (PV), and local loads. A circuit breaker (CB) enables the microgrid to connect with the main power grid and is commanded to close by the control system. Since the control command could not drive the CB, an actuator is used as shown in Fig. 1. The FOPID based microgrid central controller, as illustrated in Fig. 1, generates control signals C_1, C_2 and C_3. These signals are implemented by the control unit of each DG for voltage and frequency coordination. The description of the control strategy of the microgrid is explained in the next sections. It is worth to mention that the proposed control method is not limited to a special microgrid topology or a definite DG type because the control signals can be provided for each DG by considering the dynamic equations. The following subsections describe the dynamic models of each DG, especially PHEVs. Moreover, the control strategy of each DG including the control signals C_1, C_2 and C_3 is also demonstrated in this section.
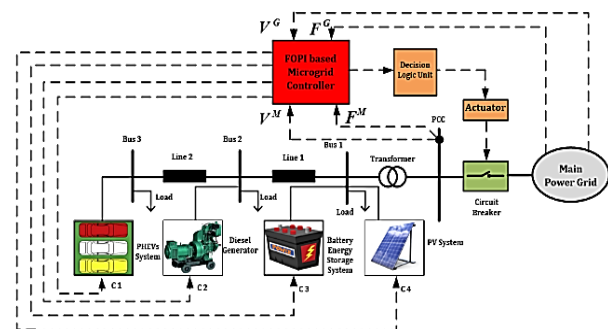

Fig. 1. Overall diagram of the microgrid with the proposed synchronization control strategy

1.2. Photovoltaic system model

The dynamic model of PV system has been described in literature such as [27-28]. Here, the model of a grid-connected PV described by Ref. [29] is considered since it is suitable for microgrid studies [29-30]. The PV array is connected to the grid through a DC/DC boost converter and a DC/AC converter (called inverter), as shown in Fig. 2. The boost converter, as indicated in Fig. 2, is controlled to extract the maximum energy from the PV array based on maximum power point tracking (MPPT) strategy. The electrical model of a PV cell is indicated in Fig. 3. As shown, V_{out}, I_{out} are the output voltage and current of each PV cell, respectively. The output current of PV cell is given as [29];

$$I_{out} = I_{PV} - I_o \left(e^{\left(\frac{V_{out}+R_S I_{out}}{V_t a}\right)} - 1 \right) - \left(\frac{V_{out}+R_S I_{out}}{R_p}\right) \quad (1)$$

Where I_{PV}, I_o are the PV cell current and saturation current, respectively, and V_t is the thermal voltage of the array, that is, $V_t = \frac{N_s k T}{q}$ in which N_s is the number of series-connected cells, q is the electron electrical charge, and T is the time constant. R_s, R_p are the series and parallel resistances, respectively. More information can be found in Ref. [29]. The MPPT controls the DC/DC boost converter and adopts the modified perturbation& observation (P&O) algorithm proposed by Ref. [31] to optimally regulate the output voltage of the PV system. This control approach uses a two-step dead beat control method to force the operating point of PV near to maximum power point (MPP). This control strategy works under the perturbations including changes in irradiation and temperature. Fig. 4 shows the performance of the 2.5 kW PV array used in the simulation studies. As shown, the PV average power follows the irradiation changes in MPPs. The changes in the average power from 0 to 0.2 s indicates the searching of algorithm to find the optimum point. When found, the PV power is set on the optimal trace and produces 2.5 kW during 0.4 to 0.6 s. Then, the irradiation decreases linearly from $25 \frac{W}{m^2}$ to $6 \frac{W}{m^2}$ and thus, the PV power falls down to 1.25 KW. After that, as demonstrated in Fig. 4, the irradiation increases linearly up to $25 \frac{W}{m^2}$ those results in increase of the PV power to 2.5 kW again. The irradiation keeps constants and however, the temperature increases to 50 degree at t = 2s. This results in a reduction in the PV power to 2.35 kW. The PV array is a set of PV cells that are connected as strings to provide the desired voltage level. The control block diagram for the DC/AC power converter (inverter) is shown in Fig. 5. The inverter operates in current control mode. The reference currents i_d^*, i_q^* are

generated using reference signals active power P^*, reactive power Q^*, frequency f^*, and voltage V^* and the correspondence measured signals P^m, Q^m, f^m, and V^m. Two other control signals, as shown in Fig. 5, are also implemented in this control scheme, that is, the signals C_1^f, C_1^V which are added to the frequency and voltage reference signals, respectively. These signals come from the optimal FOPID based microgrid central controller and acts as compensators. Notice that the control signal C_1 in Fig. 1 has been decomposed to two signals C_1^f, C_1^V. As illustrated in Fig. 5, the proportional-integral-resonance (PIR) controllers are implemented in the control system because of their robustness, good dynamic response and better reference following capability. The dynamic model of this controller is as follows;

$$G_{PIR} = \frac{2K_i \omega_c s}{s^2 + 2\omega_c s + \omega^2} \quad (2)$$

Where $K_p = 1$ is the proportional gain, $K_i = 20$ is the integral gain, $\omega = 377$ rad/sec. is the system frequency, and $\omega_c = 10$ rad/sec. is the cutoff frequency. These values have been chosen based on try and error method [32]. The frequency response of this controller is shown in Fig. 6. As demonstrated, the magnitude has an infinite peak at the resonance frequency that is the main characteristic of the resonance controllers.
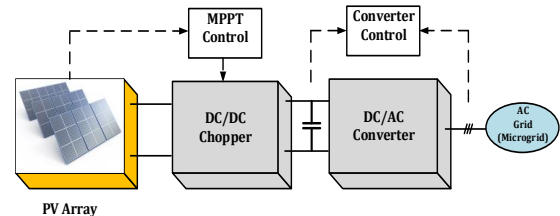

Fig. 2. A typical PV system model; the PV array is connected to grid through a DC/DC chopper and an inverter
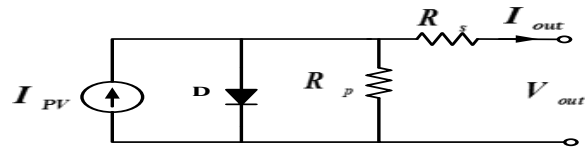

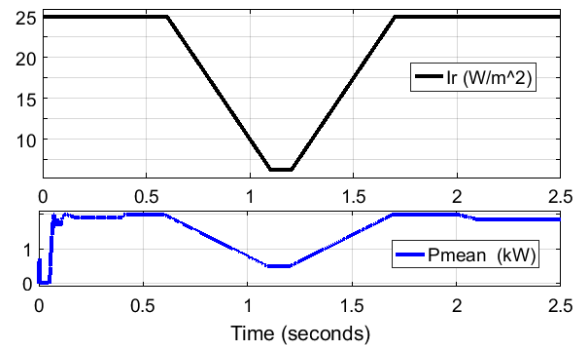**Fig. 3. Electrical model of a PV cell [29]**

Fig. 4. The average output power of PV array that follows the MPP using the modified P&O algorithm considered in simulations
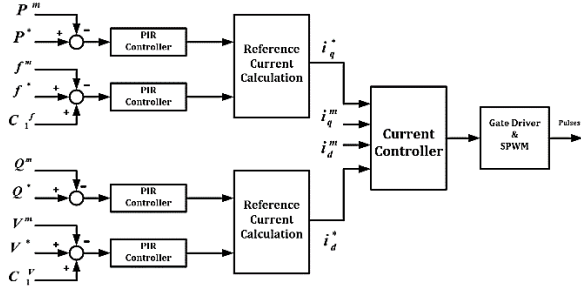
Fig. 5. Control block diagram of DC/AC converter of PV system with control compensator signals C_1^f, C_1^V and resonance controllers.
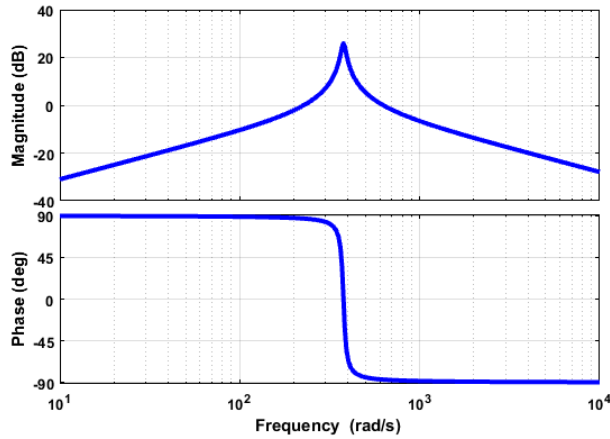

Fig. 6. Bode diagram of implemented optimal PR controllers
($K_p = 1, K_i = 20.23, \omega = 2\pi f = 377 \text{rad/sec.}, \omega_c = 10 \text{rad/sec}$)

2.2. Diesel generator model

A diesel generator is an electromechanical system and according to Fig. 7, includes two subsystems: the mechanical and the electrical subsystems. The mechanical subsystem is an internal combustion engine (ICE) that produces the mechanical torque for the electrical subsystem, i.e. the synchronous generator. Another important part of the mechanical subsystem is the speed controller, that is, the governor which takes the main role in frequency control of the diesel generator. The electrical subsystem includes the synchronous generator and the voltage control system, that is, the automatic voltage regulator (AVR) which takes the main task in voltage control of the diesel generator. These two control parts, i.e. the governor and AVR, are very important in synchronization process of the microgrid because they directly participate in frequency and voltage regulation of the microgrid. The control diagram of the diesel generator is shown in Fig. 8. Note that the control signal C_2 is also demonstrated which actually has been decomposed into two signals, i.e. C_2^ω, C_2^V. These signals are compensating signals for frequency and voltage of the diesel generator, respectively. The dynamic model of the diesel generator has been described in many papers such as [21, 33, 34] and it is as follows:

$$\dot{\delta} = \omega_0 \omega - \omega_0 \tag{3}$$

$$\dot{\omega} = -\left(\frac{D}{2H}\right)\omega + \frac{\omega_0}{2H}\left(P_{mech} - E_q' I_q^g\right) \tag{4}$$

$$\dot{E_q'} = \frac{1}{T_{do}'}\left(K_A(V_0^* - V_0) - (X_d - X_d')I_d^g\right) \tag{5}$$

$$\dot{V_0} = \frac{1}{T_R}(V_t - V_0) \tag{6}$$

The voltage at the terminal of the generator is;

$$V_t = \sqrt{\left(E_q' - X_d' I_d^g\right)^2 + \left(X_d' I_q^g\right)^2} \tag{7}$$

Where δ is angle of the rotor, ω is the rotational speed of the rotor, H is the inertia constant, T_R is the time constant of voltage regulator, T_{d0}' is the open circuit transient time constant of the direct axis, K_A is the gain of the excitation system, V^* is the reference value of the terminal output voltage, V_0 is the terminal output voltage, E_q' is the transient voltage of quadrature axis, X_d is the direct axis synchronous reactance, X_d' is the transient direct axis synchronous reactance. For other variables and constants, the reader would refer to [34].
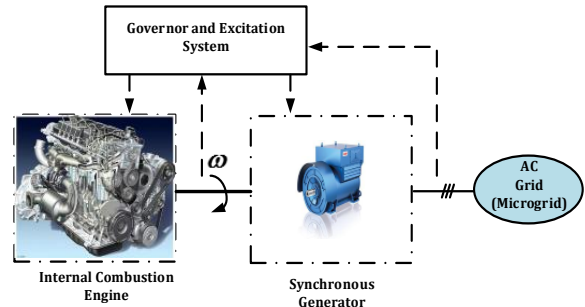

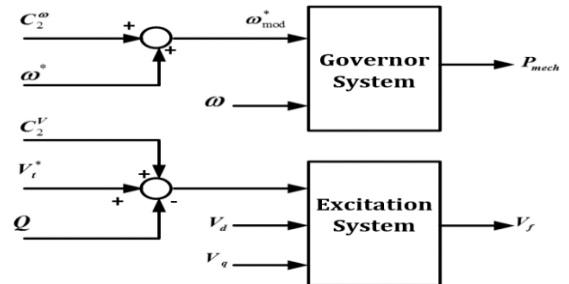**Fig. 7. Block diagram of a diesel generator; including mechanical and electrical parts**

Fig. 8. Control block diagram of diesel generator with control compensator signals C_2^ω, C_2^V

2.3. V2G Model

The plug-in hybrid electric vehicle (PHEV) has the following components: internal combustion engine (ICE), electric motor, electric generator and battery. These components operate under different control strategies. The electric motor, generator and the ICE may have been mechanically coupled in series or parallel. The ICE is coupled with the generator to produce the electrical energy to supply the electric motor. The battery is also connected in parallel with the generator and can be charged from the power grid (plug-

in feature). In this study a PHEV with series topology is considered and it is shown in Fig. 9. As it is clear from this figure, there are also two power converters that facilitate the electrical energy flow between the generator/battery and the electric motor. If the electric motor is a DC motor, the second power converter, i.e. the inverter, is avoided. However, the DC motors need more incentive care and costly. Thus, the induction motors are preferred because of their simple structure and convenience control using the power electronic based drives. The PHEV dynamic model is commonly demonstrated by a battery and a synchronous generator model. The latter was described in subsection 2.2 and is not repeated here. However, in the next section the whole PHEV model is considered for the purpose of linearization and small signal analysis. The dynamic model of lead-acid based battery that is taken from Ref. [35] is shown in Fig. 10. The equivalent model of a battery considering the effects of the parasitic distortions is shown in Fig.10 (a) while Fig.10 (b) illustrates the electrical equivalent circuit of the battery in which the resistive and capacitive real features of the battery are demonstrated. Based on electrolyte temperature, state of the charge (SOC), and current, the dynamic model of the battery can be described as follows;

$$\dot{q}_e = i_{dc}/T_s \tag{8}$$

$$\dot{i}_m = (i_{dc} - i_m)/T_m \tag{9}$$

$$\dot{\theta} = -(1/C_\theta)[P_s - (\theta - \theta_a)/R_\theta] \tag{10}$$

$$V_{dc} = E_m - V_p(q_e, i_m) + V_e e^{-\beta_e q_e} - R_0 i_{dc} \tag{11}$$

$$V_p(q_e, i_m) = \begin{cases} \frac{R_p i_m + K_p q_e}{SOC} & if \ i_m < 0 \ discharge \\ \frac{R_p i_m}{q_e + 0.1} + \frac{K_p q_e}{SOC} & if \ i_m > 0 \ charge \end{cases} \tag{12}$$

$$E_m = E_{m0} - K_e(273 + \theta)(1 - SOC) \tag{13}$$

$$R_0 = R_{00}(1 + A_0(1 - SOC)) \tag{14}$$

$$R_1 = -R_{10}(ln(DOC)) \tag{15}$$

$$R_2 = R_{20}(exp(A_{21}(1 - SOC)/(1 + \ exp(A_{22}l_m/I^*)) \tag{16}$$

$$SOC = (Q_n - Q_e)/Q_n = 1 - q_e \tag{17}$$

$$DOC = 1 - (Q_e/C(l_{ave}, \theta)) \tag{18}$$

Where V_e stands for hysteresis effects that is occur during discharging/charging process, V_m is the polarization voltage, C_θ, P_s are the thermal and power capacity of the battery, respectively, DOC is the depth of charge, R_0, R_p are the thermal and polarization resistance of the battery, respectively, θ_a is the

environment temperature, I^* is the desired current flowing through the battery, β_e is the exponential capacity factor, Q_e is the extracted capacity in Ah, Q_n is the normal capacity of the battery, $E_m, K_e, K_p, A_0, A_{21}, A_{22}$ are particular factors that are depend on the battery type. More details about the battery parameters are available in Ref. [35].

For the synchronous generator, when the PHEV is connected to the microgrid with voltage of V^m and equal reactance of X_e, Equations (3-7) are considered whereas the current components of the generator considering the constant voltage V_{dc} for the charger are;
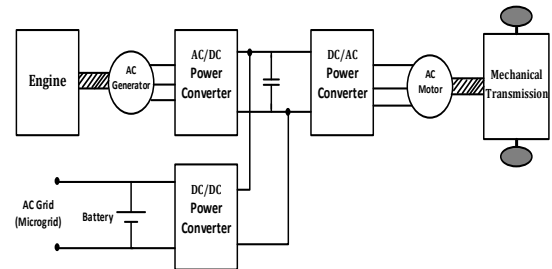

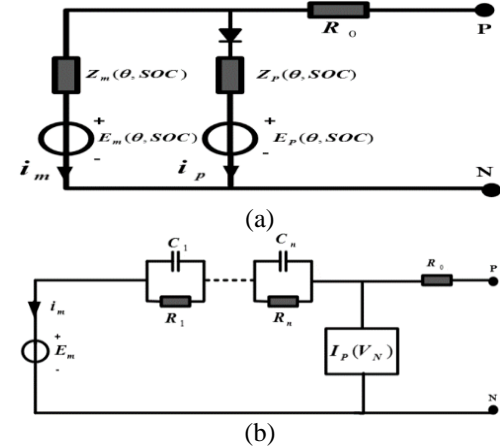**Fig. 9. Plug-in hybrid electric vehicle with series topology**

(a)

(b)

Fig. 10. PHEV battery model based on dynamic modeling of lead-acid battery proposed in Ref. [35]: (a) equivalent model with parasitic term (b) electrical circuit model
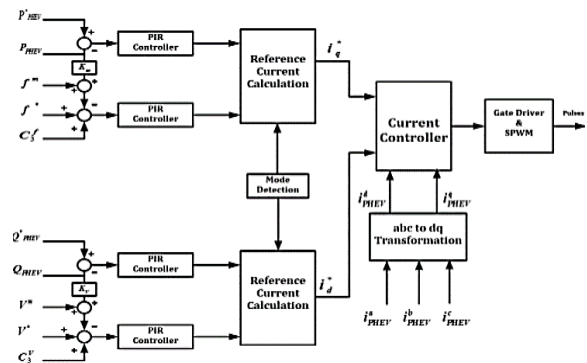

Fig. 11. Control block diagram of PHEV battery control with compensating signals C_3^f, C_3^v

$$I_d^g = -\frac{E_q'}{X_d'} + \left(\frac{V^m}{X_d' + X_e} + \frac{V_{dc}}{X_d' + X_e}\right) cos \ \delta \tag{19}$$

$$I_q^g = \left(\frac{V^m}{X_d' + X_e} + \frac{V_{dc}}{X_d' + X_e}\right) \sin \delta \qquad (20)$$

And the charger equation will be:

$$\dot{V}_{dc} = -1/C \left(\frac{E_q'}{X_d'} + \frac{V^m}{X_e} - \frac{\sqrt{\left(E_q' - X_d' I_d^g\right)^2 + \left(X_d' I_q^g\right)^2}(X_d' + X_e)}{X_d' X_e}\right) \qquad (21)$$

The control Block diagram of PHEV battery control equipped with the proposed compensation signals C_3^f, C_3^V is shown in Fig. 11. In this figure, for the sake of simplicity in the control objective, the dynamics of the DC/DC boost converter are not shown described in [36]. Actually, the DC link voltage control strategy is exerted.

3. EFFECTS OF V2G ON DYNAMICS OF MICROGRID

In this section, the effects of penetrated PHEVs on dynamics of the microgrid is evaluated. Especially, it is shown that the PHEVs have adverse effects on the microgrid voltage and power oscillations and thus they affect the synchronization process. The results are verified by linearization of the PHEV model and small signal analysis. Considering Equations (3)-(21), implementing the Taylor Series Expansion (TSE), the linearized form of PHEV dynamic model that is connected to the microgrid are as follows;

$$\dot{\Delta\delta} = \omega_0 \Delta\omega \qquad (22)$$

$$\dot{\Delta\omega} = -\frac{D}{2H}\Delta\omega + \frac{\omega_0}{2H}\left(-E_{q0}'\Delta I_q^g - I_{q0}^g \Delta E_q'\right) \qquad (23)$$

$$\dot{\Delta E_q'} = 1/T_{d0}'\left(-K_A \Delta V_0 - (X_d - X_d')\Delta I_d^g\right) \qquad (24)$$

$$\dot{\Delta V_0} = 1/T_R(\Delta V_t - \Delta V_0) \qquad (25)$$

$$\dot{\Delta V_{dc}} = (1/CX_d')\Delta E_q' - \left(\frac{X_e + X_d'}{X_d' X_e}\right)\Delta V_t \qquad (26)$$

$$\dot{\Delta I_m} = 1/T_m Z_R \left(\left(1 - R_0 + \frac{R_0 A_1 Q_e}{K_c CI^*}\right)\Delta V_{dc} + \left(\frac{R_0 A_1 V_{dc}}{K_c CI^*} + \frac{K_e(\theta + 273)}{K_c CI^*}\right)\Delta Q_e - \Delta I_m Z_R + \left(\frac{K_e \theta_e}{K_c CI^*}\right)\Delta\theta\right) \qquad (27)$$

$$\dot{\Delta Q_e} = -\left(1 - R_0 + \frac{R_0 A_1 Q_e}{K_c CI^*}\right)\Delta V_{dc} + \left(\frac{R_0 A_1 V_{dc}}{K_c CI^*} + \frac{K_e(\theta + 273)}{K_c CI^*}\right)\Delta Q_e + \left(\frac{K_e \theta_e}{K_c CI^*}\right)\Delta\theta \qquad (28)$$
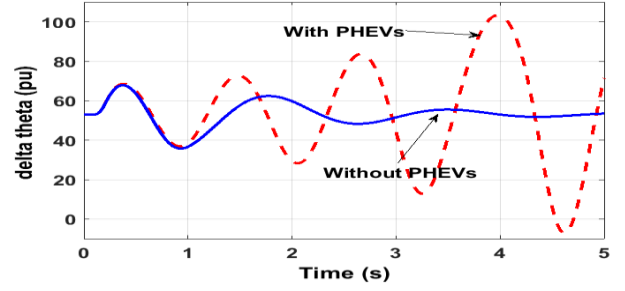
$$\dot{\Delta\theta} = 1/C_0(1 - 1/R_0)\Delta\theta \qquad (29)$$

$$\Delta I_d^g = -\left(E_{q0}'/X_d'\right)\Delta E_q' - \left(\frac{V^m \sin\delta_0}{X_d' + X_e} - \frac{V_{dc0} \sin\delta_0}{X_d' + X_e}\right)\Delta\delta + \frac{V_{dc0} \cos\delta_0}{X_d' + X_e}\Delta V_{dc} \qquad (30)$$
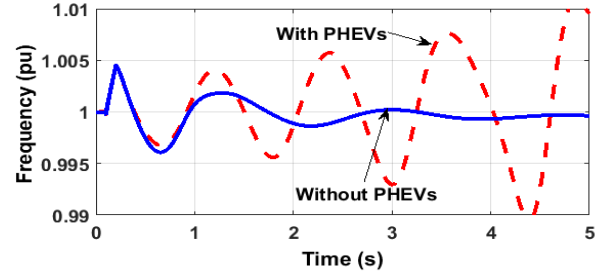
$$\Delta I_q^g = \left(\frac{V^m \cos\delta_0}{X_d' + X_e} + \frac{V_{dc0} \cos\delta_0}{X_d' + X_e}\right)\Delta\delta + \frac{V_{dc0} \sin\delta_0}{X_d' + X_e}\Delta V_{dc} \qquad (31)$$

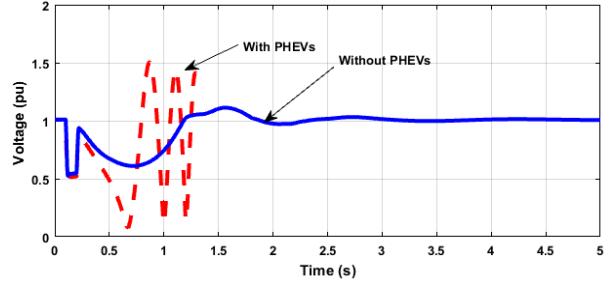Thus, these Equations describe the linearized model can be presented with the standard form as follow;

$$\dot{\Delta x}(t) = A\Delta x(t) + Bu(t) \qquad (32)$$

(a)

(b)

(c)

Fig. 12. Effects of PHEVs on the microgrid dynamic response when a L-L fault occurs at the PCC bus.
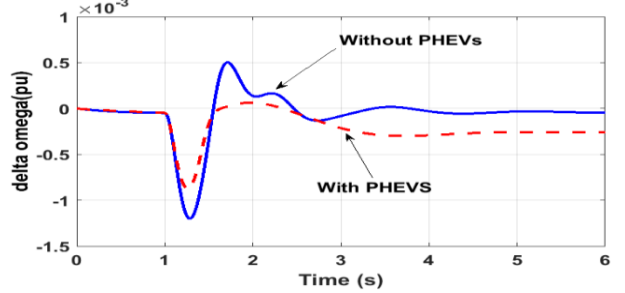

Fig. 13. Effects of PHEVs on the microgrid dynamic response when a L-G fault occurs at the PCC bus.

Where A is the state matrix of the linear system, $x(t)$ is the state vector of the system, and $u(t)$ is the input that is set to be zero for small signal stability analysis. From the system operating point acquired from the power flow analysis, the elements of the state matrix A can be obtained and are given in Annex A. After linearization and using the parameters given in Annex B, the eigenvalues of the system containing PHEVs are given in Table 1. To make the effects of PHEVs clearer on the dynamic model, the system eigenvalues considering constant loads (without PHEVs) are given in this Table, too. It is obvious from the eigenvalues that the system suffers from low frequency oscillations when

the PHEVs are connected. This makes the microgrid vulnerable to the system fault and also switching actions such as synchronization. Also, this oscillation makes the damping time (settling time) of the microgrid power and frequency oscillation longer and thus the process of synchronization gets too much time or even fail. For the purpose of clearness, the simulation results are provided for two cases when a fault is occurred in the PCC bus of the microgrid and the results are shown in Figs. 12-13. The faults are considered as line-to-line (LL) fault and line-to-ground (LG) fault. It is clear from these figures that the microgrid frequency and voltage could not keep the stability margins.

Thus, it can be concluded that PHEVs impose low frequency oscillation on the microgrid dynamics that cause the considerable fluctuations in the voltage and frequency of the microgrid. These effects are more notable because of low-inertia dynamic feature of the microgrid model and, as a matter of fact, one must consider these oscillations due to synchronization process so that the coordinated control of DGs is able to damp these fluctuations rapidly and also provides the microgrid with robust stability during faults too.

Table 1. Microgrid eigenvalues considering PHEVs in dynamic model

Eigenvalue: $\alpha \pm j\beta$	
Without PHEVs (constant loads)	With PHEVs
-0.2341	0
-11.372	-5.20
-0.2563+j7.880	-0.25+j15.82
-0.2563-j7.880	-0.25-j15.82
-12.364	-12.66
-	-0.513+j7.32
-	-0.513-j7.32
-	-3.34

4. PROPOSED MICROGRID CONTROL SCHEME

4.1. Proposed FOPID based microgrid central controller

The proposed FOPID based microgrid central controller is the key element in control strategy of the microgrid which was shown in Fig. 1. The central controller generates the command offsets to regulate the voltage and frequency of each DG so that the voltage and frequency of the microgrid coordinate with those of the main grid. The structure of the proposed microgrid central controller is indicated in Fig. 14. The microgrid frequency f^m and main grid frequency f^G are determined using phase-locked-loops (PLLs). The frequency error e_f is given the optimal fractional order PID (FOPID) controller. The process of design of this controller will be described in the following subsection. The output signal of this controller

is given to weighting functions WF_i ($i = 1 \dots 3$) in order to generate the compensation frequency signals C_1^f, C_2^ω, C_3^f. Note that C_2^ω is also compensation frequency signal since $\omega = 2\pi f$. This signal is considered as a factor of ω instead of frequency f in order to cope the diesel generator dynamics directly. In a similar way, the voltages of the microgrid V^m and the main grid V^G are measured and compared. The voltage sequence analyzers are used to determine the correct sequence of these voltages. The voltage error e_V is given to the optimal FOPID controller and the output signal is given to the weighting functions WF_i ($i = 4 \dots 6$) to produce the compensation voltage signals C_1^V, C_2^V, C_3^V. The weighting functions WF_i ($i = 4 \dots 6$) are the same as weighting functions WF_i ($i = 1 \dots 3$). Both frequency and voltage compensation signals are sent for DGs to regulate the voltage and frequency of these resources to damp the voltage and power oscillations rapidly in the microgrid and set to the main grid. The voltage and frequency errors are sent to the Decision Logic Unit (DLU), shown in Fig. 15, to check the synchronization criterions. When these errors are minimized, namely smaller than a predetermined threshold T_V, T_f, then the DLU commands the actuator to close the circuit breaker. Thus, the proposed control strategy makes the synchronization process swift, soft and safe. The weighting functions have been chosen and optimally obtained using the MATLAB Optimization Tools [37] based on Trust Region Reflective Algorithm (TRRA) and are as follows:

$$WF_1 = WF_4 = \frac{0.19s + 0.38}{s + 0.38}$$

(33)

$$WF_2 = WF_5 = \frac{0.65s^3 + 19.50s^2 + 837.70s + 5029}{s^3 + 22.80s^2 + 1117s + 43.20}$$

(34)

$$WF_3 = WF_6 = \frac{0.93s^3 + 11.63s^2 + 471.40s + 9891}{s^3 + 2.45s^2 + 988.80s + 385.70}$$

(35)

These weighting functions are proper transfer functions in's' domain and their frequency responses are indicated in Figs. 16-18.
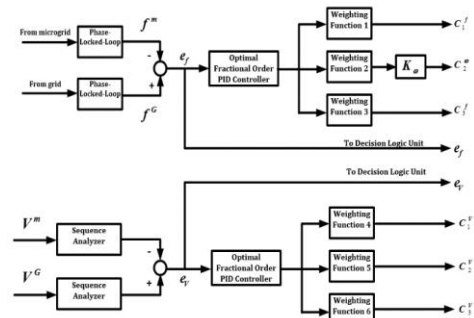

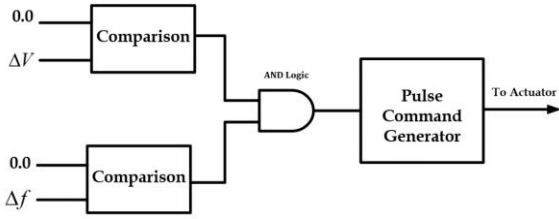
Fig. 14. Proposed FOPI based microgrid central controlle

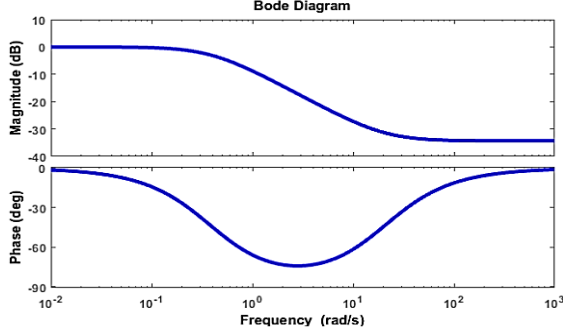Fig. 15. Decision logic unit (DLU) in the proposed control strategy

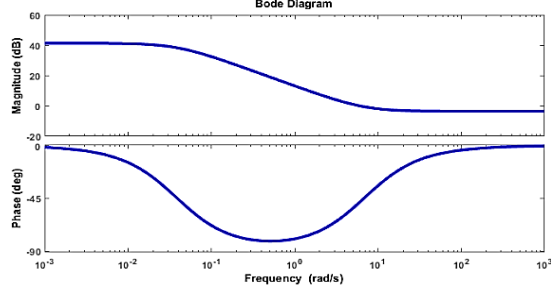Fig. 16. Frequency response of the weighting functions 1, 4 (WF_1, WF_4)

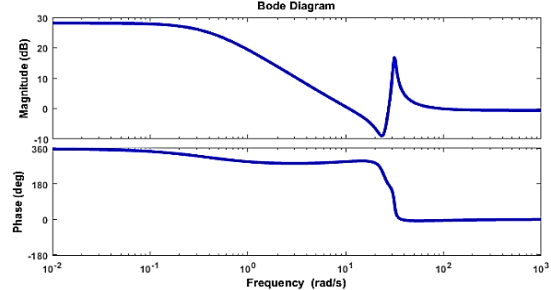Fig. 17. Frequency response of the weighting functions 2, 5 (WF_2, WF_5)

Fig. 18. Frequency response of the weighting functions 3, 6 (WF_3, WF_6)

4.2. Designing the optimal fractional order PID (FOPID) controller based on GA algorithm

Tuning of conventional PID controllers has been the subject of many control application researches. Nowadays, implementing the fractional calculus in electric power engineering applications has getting more attention, for example see Refs. [38-39]. The FOPID controllers introduce more freedom of degrees in designing process by rendering not integer orders for derivative and integral parts of the conventional PID controllers. The purpose of this section is to design the optimal FOPID controller embedded in the microgrid central controller (MCC).

4.2.1. Fractional order-based systems preliminaries

The fractional order concept is an expansion of the integer order differentiator based classic systems. The main operator of fractional calculus is given as [40];

$$_aD_t^\beta = \begin{cases} \frac{d^\beta}{dt^\beta} & \beta > 0 \\ 1 & \beta = 0 \\ \int_a^\beta (d\tau)^\beta & \beta < 0 \end{cases} \tag{36}$$

Where a, t are the operation border, and β is the non-integer order. In this study, Caputo definition [40] is used because of its soft derivative action;

$$_aD_t^\beta f(t) = \begin{cases} \frac{1}{\Gamma(m-\beta)} \int_a^t \frac{f^m(\tau)}{(t-\tau)^{\beta-m+1}} & m-1 < \beta < m \\ \frac{d^m}{dt^m} f(t) & \beta = m \end{cases} \tag{37}$$

If the integral of the non-integer derivative $_aD_t^\beta$ of function $f(t)$ derived, then [40];

$$_aD_t^{-\beta} \left(_aD_t^\beta f(t) \right) = f(t) - \sum_{i=1}^k \left(_aD_t^{\beta-i} f(t) \right) \frac{(t-a)^{\beta-i}}{\Gamma_{t=a}(\beta-i+1)} \tag{38}$$

Where, $k-1 < \beta < k$. The non-integer integral operator $_aD_t^{-\beta}, \beta > 0$, is bounded so that the following Euclidian norm is adopted [40];

$$\left\| _aD_t^\beta f(t) \right\|_p \le \kappa \|f(t)\|_p \tag{39}$$

Where, $0 < p < \infty$, $0 < \kappa < \infty$. In these equations, $\Gamma(.)$ represents the Gamma function, that is;

$$\Gamma(\gamma) = \int_0^\infty t^{\gamma-1} e^{-t} \, dt \tag{40}$$

The stability of the fractional order systems has been declared in many researches such as [39]-[40]. According to Theorem stated in [40], a fractional order system of the form $_0D_t^\beta \zeta = A\zeta, \zeta(0) = \sigma$, where σ is a constant, is asymptotically stable if;

$$|eig(A)| \ge \frac{\beta\pi}{2} \tag{41}$$

And each element of the states reduces to zero such as $t^{-\beta}$. Thus, the system keeps stability margins if it is asymptotically stable or the critical eigenvalues of matrix A satisfy the criterion (40). More details about fractional calculus would be found in [40].

4.2.2. FOPID controller and optimal tuning based on GA

The general structure of a fractional order PID controller is as follows;

$$K(s) = K_p + \frac{K_i}{s^{\beta_i}} + K_d s^{\beta_d} \tag{42}$$

Where K_p, K_i, K_d are, respectively, the proportional, integral, and derivative gains of the FOPID controller and β_i, β_d are non-integers dedicated to the integral and derivative parts, respectively. It should be noted that, the two FOPID controllers in the microgrid shown in Fig. 1 are the same. Each FOPID controller has five

parameters as K_p, K_i, K_d and β_i, β_d. To tune the FOPID parameters optimally, the GA is used. For this purpose, the objective function that must be minimized is defined as the integral of time multiply absolute error (ITAE) of deviation of the voltage and frequency of the microgrid respected to the main grid, i.e. the cost function is;

$$J = \int_0^\infty t(|\Delta V| + |\Delta f|)dt \qquad (43)$$

Constrained to;

$$K_p^{min_p^{max}}, K_i^{min_i^{max}}, K_d^{min_d^{max}}, \beta_i^{min_i^{max}}, \beta_d^{min_d^{max}} \qquad (44)$$

Where $\Delta V, \Delta f$ actually are the voltage error e_v and frequency error e_f, respectively, indicated in Fig. 14. Thus, the objective of the optimization problem is to find the parameters of controller K such that the voltage and frequency errors are minimized. The flowchart of the implemented GA is shown in Fig. 19. In order to acquire better performance, population size, number of chromosomes, mutation rate, and mating rate were chosen as 80, 4, 10%, and 50%, respectively.
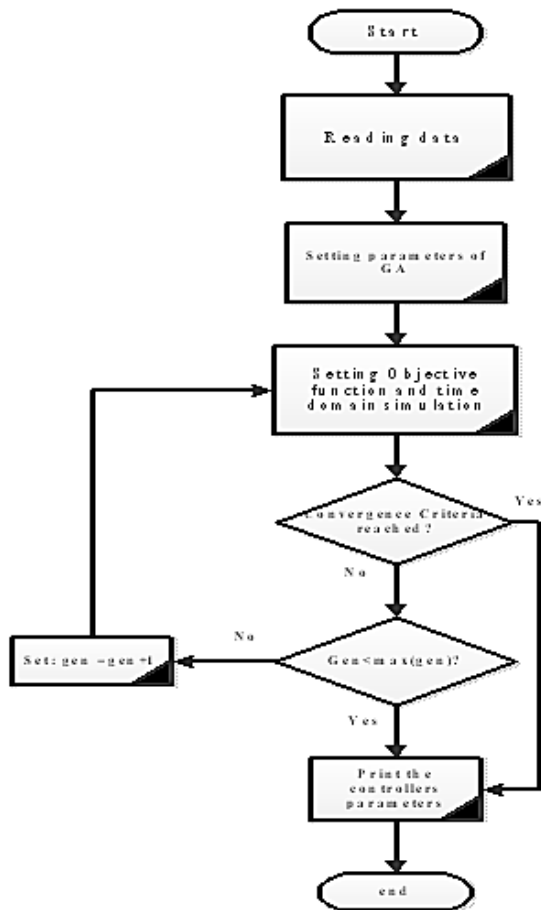

Fig. 19. Flowchart of optimal tuning process of FOPID controller parameters using GA

The optimized FOPID controller parameters are obtained as;

$$K_p = -1.235, K_i = -1, K_d = 0.534, \beta_1 = 0.623, \beta_2 = 0.567$$

Thus, the FOPID is optimally tuned and is implemented in the simulation studies presented in the next section. The algorithm has reached convergence after 23 iterations.

5. SIMULATION RESULTS

The performance of the proposed optimal FOPID based synchronization control scheme is evaluated through simulations in MATLAB/SIMULINK [37]. For comparison objectives, the performance of the robust control based synchronous strategy developed in Ref. [21] is also evaluated. The microgrid model is shown in Fig. 1. The microgrid is PHEV-dominant to demonstrate the effects of PHEVs on synchronization process. The rated power of PHEVs is 12 kW while the rated powers of diesel generator and PV system are 6 kW and 2.5 kW, respectively. The parameters of the PHEV, PV and the diesel generator are given in Annex A. The microgrid loads are constant with mostly inductive characteristic. Two cases studies have been considered. In the first case, the effect of delay of communication links on the synchronization process is verified. In the second case, besides of considering the delay, the effect of changing the line resistance is also considered. The simulations are done for the two methods in the same conditions to make a proper comparison. In all results, 'Robust Method [21]' stands for the strategy described in Ref. [21] and 'Proposed FOPID' denotes the proposed optimal fractional order PID based control strategy.
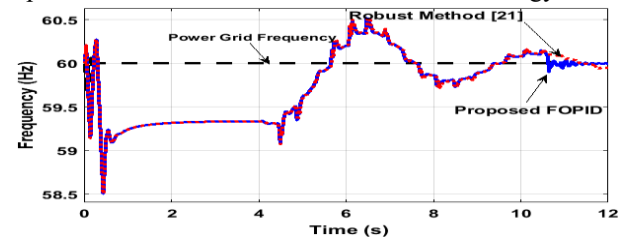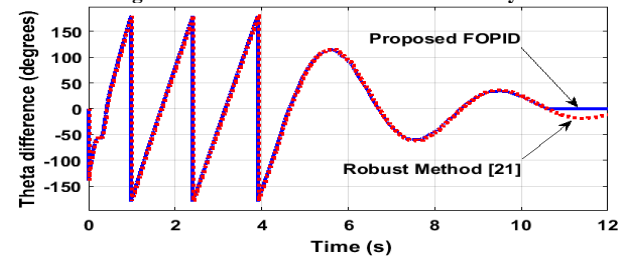

Fig. 20. Case I: 500 ms communication delay

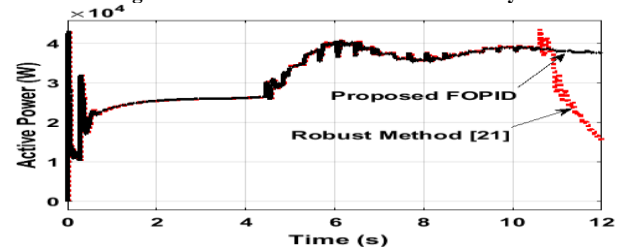

Fig. 21. Case I: 500 ms communication delay

Fig. 22. Case I: 500 ms communication delay

5.1. Effects of delay in communication links on synchronization process

In this case, 500 ms delay in the communication links is considered and the microgrid is equipped with the two control methods separately. Figs. 20-25 illustrate the simulation results. Fig. 20 shows that, by implementation of the proposed FOPID control strategy, the microgrid frequency matches the power grid frequency softly than the robust control method of [21]. The angle oscillation, as shown in Fig. 21, goes rapidly toward zero using the proposed method. Fig. 22 shows that the PV active power has lower distortion and is able to track its control power points quicker than the robust method [29]. The active power of the diesel generator reaches to its nominal value, i.e. 6 kW, more rapidly than the robust method, as demonstrated in Fig. 23. The same conclusion can be presented for active power of PHEVs as illustrated in Fig. 24. The compensating signals, as shown in Fig. 25, are generated to relief the power oscillations of the generation systems. As expected, these signals strengths are proportional to the rated power of the generation resources so that the compensating signal for PHEVs has the largest amplitude because the microgrid, as mentioned before, is PHEV-dominant.
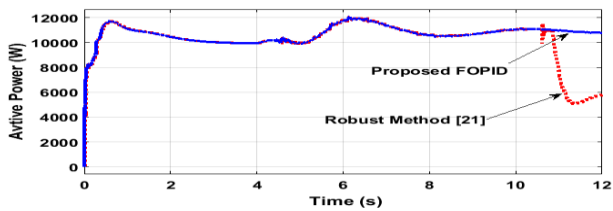
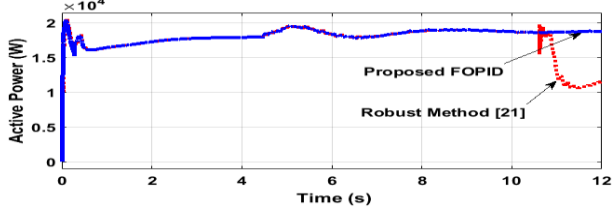**Fig. 23. Case I: 500 ms communication delay**
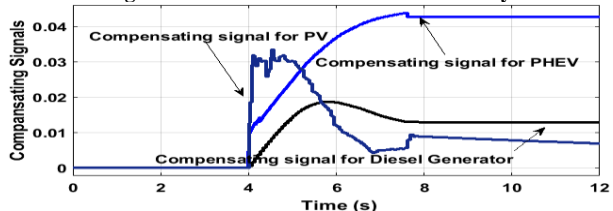
Fig. 24. Case I: 500 ms communication delay

Fig. 25. Case I: 500 ms communication delay

Fig. 26. Case II: 64 ms communication delay and 15% changes in resistance of line 1

Fig. 27. Case II: 64 ms communication delay and 15% changes in resistance of line 1
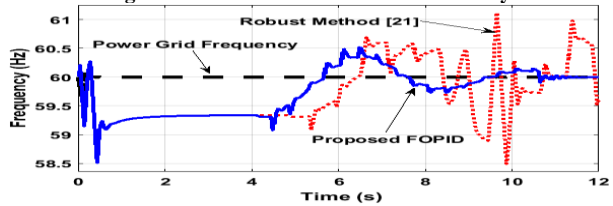
Fig. 28. Case II: 64 ms communication delay and 15% changes in resistance of line 1
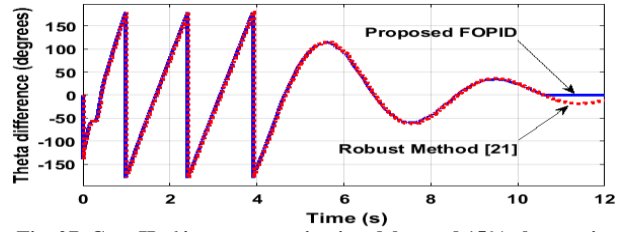
Fig. 29. Case II: 64 ms communication delay and 15% changes in resistance of line 1
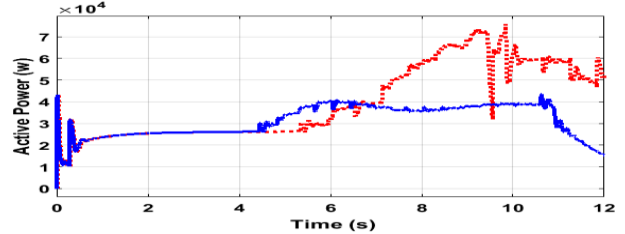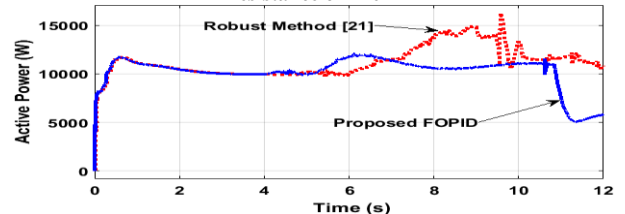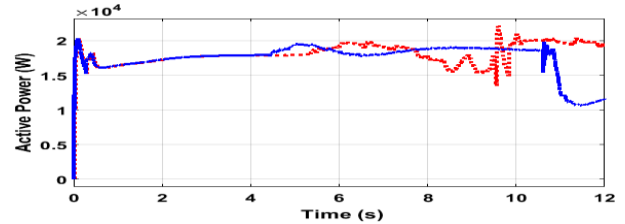
Fig. 30. Case II: 64 ms communication delay and 15% changes in resistance of line 1

Fig. 31. Case II: 64 ms communication delay and 15% changes in resistance of line 1

5.2. Effects of 15% changes in transmission line 1 and 64 ms delay in communication links simultaneously on synchronization process

To study the parameter variation effects on the synchronization process and to confirm the robustness of the proposed control strategy, resistance of transmission line1 of the microgrid, which is demonstrated in Fig. 1, is changed by 10% during the simulation and 64 ms communication delay in communication links is also implied simultaneously. The results are shown in Figs. 26-31. Fig. 26 illustrates that the proposed FOPID control strategy is able to synchronize the microgrid with the main power grid

successfully whereas the synchronization process is failed when the robust method of [21] is employed. Fig. 27 confirms this issue by illustrating of the angle oscillation. The active powers of PV system, diesel generator, and PHEVs, as shown in Figs. 28-30, are oscillatory when the robust method is exerted but these oscillations are relieved when the proposed FOPID control scheme is used. The compensating signals generated by the proposed FOPID based microgrid central controller are shown in Fig. 31. As it is clear, the signals are generated to reduce the oscillations when they are implied to the control system of each distributed resources.

6. CONCLUSION

This study described a synchronization strategy for microgrid using a centralized optimal fractional order control scheme. The FOPID was optimally tuned using the genetic algorithm (GA). The effects of V2G on the microgrid dynamic behaviour as well as synchronization process were investigated. By increasing the number of PHEVs, the oscillations in the voltage and frequency of the microgrid also increase. The simulation results validated the effectiveness and robustness of the proposed control strategy.

Appendix A.

The elements of matrix A of the linearized system, where $e_{ij}, i, j = 1…6$ is the element of the matrix. Note that A is a square matrix and here only the nonzero elements are given as follows;

$$e_{11} = e_{13} = e_{16} = 0$$

$$e_{21} = -\frac{\omega_{s0} E'_{q0}}{2H}\left(\frac{V^m \cos\delta_0}{X'_d + X_e} + \frac{V_{dc0}\cos\delta_0}{X'_d + X_e}\right)$$

$$e_{23} = -\frac{\omega_{s0}}{2H} I^g_{q0}$$

$$e_{26} = -\frac{\omega_{s0} E'_{q0}}{2H}\left(\frac{V_{dc0}\sin\delta_0}{X'_d + X_e}\right)$$

$$e_{31} = \frac{(X'_d - X_d)}{T'_{do}}\left(\frac{V^m \sin\delta_0}{X'_d + X_e} + \frac{V_{dc0}\sin\delta_0}{X'_d + X_e}\right)$$

$$e_{33} = \frac{E'_{q0}}{X'_d}\left(\frac{(X'_d - X_d)}{T'_{do}}\right) - \frac{1}{T'_{do}}$$

$$e_{36} = -\left(\frac{(X'_d - X_d)}{T'_{do}}\right)\frac{E'_{q0}\cos\delta_0}{X'_d + X_e} \quad e_{41} = \left(\frac{E'_{q0}X'_d - X'^2_d I^g_{d0}}{T_R V_{t0}}\right)\left(\frac{V^m \sin\delta_0}{X'_d + X_e} + \frac{V_{dc0}\sin\delta_0}{X'_d + X_e}\right) + \left(\frac{X'^2_d I^g_{d0}}{T_R V_{t0}}\right)\left(\frac{V^m\cos\delta_0}{X'_d + X_e} + \frac{V_{dc0}\cos\delta_0}{X'_d + X_e}\right)$$

$$e_{43} = \left(\frac{E'_{q0} - X'_d I^g_{d0}}{T_R V_{t0}}\right) + \left(\frac{E'_{q0}X'_d - X'^2_d I^g_{d0}}{T_R V_{t0}}\right)\left(\frac{E'_{q0}}{X'_d}\right)$$

$$e_{45} = -\left(\frac{E'_{q0}X'_d - X'^2_d I^g_{d0}}{T_R V_{t0}}\right)\left(\frac{V_{dc0}\cos\delta_0}{X'_d + X_e}\right) + \left(\frac{X'^2_d I^g_{d0}}{T_R V_{t0}}\right)\left(\frac{V_{dc0}\sin\delta_0}{X'_d + X_e}\right)$$

Appendix B

Parameters of the microgrid, which is used in this study, are as follows;

Diesel generator:

Ratings: 6 kW, 380/220 V, 3Φ 4 wire, 1800 r/min, 60 Hz, with brushless self-excited excitation system.

PV system:

Rating: 2.5 kW, $V_s = 400$ V, Output filter inductance of the inverter system = 1 mH, Output Filter capacitance of the inverter system = 20 μF, Output filter resistance of the inverter system = 0.2 Ω. For more details about PV model please refer to Ref. [29].

PHEVs:

The PHEVs are considered as lumped and parked in a parking lot that works under a unique control strategy to be connected to the power grid (V2G and G2V technologies). Total power specification of the PHEVs are as follows;

Rated total power 12 kW produced by 4 PHEVs with each rated power 3kW. The detailed battery parameters are given in Ref. [35].

REFERENCES

[1] B. Shalali and G. Shahgholian, "Design and analysis of a fast and robust SMC controller with multi-slope sliding surface for three-level NPC single phase inverter for various loads and the reduction", *Iran. J. Electr. Comput. Eng.*, vol. 55, 2017.

[2] H. Alipour et al., "Asymptotical stability of four-wheel electric vehicle using a three-layer and SMC controller", *Iran. J. Electr. Comput. Eng.*, vol. 43, 2015.

[3] M. Veisi et al, "Designing of a robustly stable optimal fuzzy controller for stabilizing speed of electric vehicle in presence of parametric uncertainties and external disturbances", *Iran. J. Electr. Comput. Eng.,* vol. 10, 2019.

[4] M. Barnes et al, "Real-world microgrid: an overview", *in Proc. IEEE Int. Conf. Syst. Eng.*, pp. 1-8., 2007.

[5] M. Vallem, D. Jensen and J. Mitra, "Reliability evaluation and need based storage assessment for surety microgrids", *Proc. North Amer. Power Syms.*, 2006.

[6] P. Mercier, R. Cherkaoui and A. Oudalov, "Optimizing a battery energy storage system for frequency control application in an isolated power system", *IEEE Trans. Power Syst.*, vol. 24, pp. 1469-1477, 2009.

[7] H. Hwang and L. Gilbert, "Synchronization of wind turbine generators against an infinite bus under gusting wind conditions", *IEEE Trans. Power Appl. Syst.*, vol. 97, pp. 536-544, 1978.

[8] Y. Yang, G. Shang and Y. Fang, "A fast following synchronizer of generators", *IEEE Trans. Energy Conv.*, vol. 3, pp. 765-769, 1988.

[9] L. Gross, L. Anderson and R. Young, "Avoid generator and system damage due to a slow synchronizing breaker", *in Proc. 24th Annu. Western Protective Relay Conf.*, pp. 1-20, 1997.

[10] R. Evans, "Amanual/automatic synchronization circuit for a 37.5MVA steam-turbine-driven generator", *IEEE Trans. Ind. Appl.*, vol. 26, pp. 1081-1085, 1990.

[11] N. Stringer, "Voltage considerations during generator synchronizing," *IEEE Trans. Ind. Appl.*, vol. 35, pp. 526-529, 1999.

[12] C. Jin, M. Gao, X. Lv and M. Chen, "A seamless transfer strategy of islanded and grid-connected mode switching for microgrid based on droop control, "*IEEE Energy Convers. Congress Exposition*, pp. 969-973, 2012.

[13] T. Sezi, "A new method for measuring power system frequency", *IEEE Conf. Distrib.*, pp. 400-405, 1999.

[14] M. Begovic, P. Djuric, S. Dunlap and A. Phadke, "Frequency tracking in power networks in the presence of harmonics", *IEEE Trans. Power Delivery*, vol. 8, pp. 480-486, 1993.

[15] J. Yang and C. Liu, "A precise calculation of power system frequency and phasor", *IEEE Trans. Power Delivery*, vol. 15, pp. 494-499, 2000.

[16] C. Cho et al., "New ideas for a soft synchronizer applied to CHP cogeneration", *IEEE Trans. Power Delivery*, vol. 26, pp. 11-26, 2011.

[17] J. Simpson, F. Dörfler and F. Bullo, "Synchronization and power sharing for droop-controlled inverters in islanded microgrids", *Int. Federation Autom. Control*, vol.49, pp. 2603-2611, 2013.

[18] A. Bellini, S. Bifaretti and F. Giannini, "A robust synchronization method for centralized microgrids", *IEEE Trans. Ind. Appl.*, pp. 4587-94, 2014.

[19] C. Cho et al., "Active synchronizing control of a microgrid", *IEEE Trans. Power Electron.*, vol. 26, pp. 3707-19, 2011.

[20] J. Giraldo, E. Nava and N. Quijano, "Synchronization of isolated microgrids with a communication infrastructure using energy storage systems", *Int. J. Electr. Power Energy Syst.*, vol. 63, pp. 71-82, 2014.

[21] S. Taher, M. Zolfaghari, C. Cho and M. Shahidehpour, "A new approach for soft synchronization of microgrid using robust control theory", *IEEE Trans. Power Delivery*, vol. 32, pp. 1370-1381, 2017.

[22] S. Coman et al., "Fractional order control for DC electrical drives in networked control systems", 12th *Int. Conf. Optim. Electr. Electron. Equip.,* 2010.

[23] S. Ratrout et al., "Optimization methods in fractional order control of electric drives: A comparative study", *10th Int. Symp. Mechatronics its Appl.*, 2015.

[24] E. Sahin et al., "A PSO optimized fractional-order PID controller for a PV system with DC-DC boost converter", *Power Electron. Motion Control Conf. Exposition*, 2014.

[25] S. Taher et al., "Fractional order PID controller design for LFC in electric power systems using imperialist competitive algorithm", *Ain Shams Eng. J., vol.* 5, pp. 121-135, 2014.

[26] I. Pan et al., "Frequency domain design of fractional order PID controller for AVR system using chaotic multi-objective optimization", *Int. J. Electr. Power Energy Syst.*, vol. 51, pp. 106-118, 2013.

[27] M. Wanik et al., "Simplified dynamic model of photovoltaic generation system for grid integration studies", *5th Int. Conf. Intell. Adv. Syst.*, 2014.

[28] M. Saadawi et al, "A proposed dynamic model of photovoltaic-DG system", *Proc. 1st Int. Nucl. Renewable Energy Conf.,* 2010.

[29] M. Villalva et al., "Comprehensive approach to modeling and simulation of photovoltaic arrays", *IEEE Trans. Power Electron.,* vol. 24, 2009.

[30] E. Muljadi, M. Singh and V. Gevorgian, "User guide for PV dynamic model simulation written on PSCAD platform", www.nrel.gov/publications.

[31] G. Dileep and S. Singh, "Maximum power point tracking of solar photovoltaic system using modified perturbation and observation method", *Renewable Sustain. Energy Rev.,* vol. 50, pp. 109-129. 2015.

[32] R. Teodorescu, F. Blaabjerg, M. Liserre and P. Loh, "Proportional-resonant controllers and filters for grid-connected voltage-source converters", *IEEE Proc. Electr. Power Appl.,* vol. 153, 2006.

[33] M. Karrari and O. Malik, "Identification of heffron-hillips model parameters for synchronous generators using online measurement," *IEEE Proc. Gener., Transm. Distrib.*, vol. 151, pp. 313-320, 2004.

[34] P. Kundor, "Power system stability and control", McGraw Hill, pp. 780-808, 1994,

[35] M. Ceraolo, "New dynamical models of lead–acid batteries", *IEEE Trans. Power Syst.*, vol. 15, 2000.

[36] J. Gissing et al., "Optimal control of series plug-in hybrid electric vehicles considering the cabin heat demand", *IEEE Trans. Control Syst. Technol.*, vol. 24, 2016.

[37] The Mathworks, "MATLAB/SIMULINK", Release 9.1.0.44, 2016.

[38] L. Chaib et al., "Optimal design and tuning of novel fractional order PID power system stabilizer using a new metaheuristic Bat algorithm", *Ain Shams Eng. J.,* vol. 8, pp. 113-125, 2017.

[39] P. Kumar et al., "Optimal design of robust FOPID for the flight control system using multi-objective differential evolution", *Proc. RAECS UIET Panjab Univ. Chandigarh,* 2015.

[40] Podlubny, "Fractional Differential Equations", Academic Press, San Diego, 1999.

[41] A. Khorshidi, M. Zolfaghari and M. Hejazi, "Dynamic modeling and simulation of microturbine generating system for stability analysis in microgrid networks", *Int. J. Basic Sci. Appl. Res.*. vol. 3, pp. 663-670, 2014.

[42] M. Zolfaghari et al., "A fractional order proportional-integral controller design to improve load sharing between DGs in microgrid", *Smart Grids Conf.*, 2016.

[43] M. Zolfaghari et al., "A model predictive control based virtual active power filter using V2G technology", *Int. J. Electr., Comput., Energetic, Electron. Commun. Eng.,* vol. 11, pp. 954-962, 2017.

[44] M. Zolfaghari, G. Gharehpetian and M. Abedi, "A repetitive control-based approach for power sharing among boost converters in DC microgrids", J. Oper. Autom. Power Eng., vol. 7, pp. 168-175, 2019.

[45] F. Babaei and A. Safari, "SCA based fractional-order PID controller considering delayed EV aggregators", J. Oper. Autom. Power Eng., vol. 8, pp. 75-85, 2020.

[46] H. Radmanesh and M. Saeidi, "Stabilizing microgrid frequency by linear controller design to increase dynamic response of diesel generator frequency control loop", J. Oper. Autom. Power Eng., vo. 7, pp. 216-226, 2019.